Single-molecule dynamics reflects IgG conformational changes associated with ion-exchange chromatography

Anastasiia Misiura[a], Hao Shen[b], Lawrence Tauzin[a], Chayan Dutta[a], Logan D.C. Bishop[a], Nicole C. Carrejo[a], Jorge Zepeda O[c], Shahryar Ramezani[d], Nicholas A. Moringo[a], Amanda B. Marciel[d], Peter J. Rossky[ade], Christy F. Landes[acde]*

[a]Department of Chemistry, [c]Department of Electrical and Computer Engineering, [d]Chemical and Biomolecular Engineering, [e]Smalley-Curl Institute, Rice University, 6100 Main St, Houston, Texas 77005, United States

[b]Department of Chemistry and Biochemistry, Kent State University, 800 E Summit St, Kent, Ohio 44240, United States

* Corresponding Author: cflandes@rice.edu

Abstract:

Conformational changes of antibodies and other biologics can decrease the effectiveness of pharmaceutical separations. Hence, a detailed mechanistic picture of antibody-stationary phase interactions that occur during ion-exchange chromatography (IEX) can provide critical insights. This work examines antibody conformational changes and how they perturb antibody motion and affect ensemble elution profiles. We combine IEX, three-dimensional single-protein tracking, and circular dichroism (CD) spectroscopy to investigate conformational changes of a model antibody, immunoglobulin G (IgG), as it interacts with the stationary phase as a function of salt conditions. The results indicate that absence of salt enhances electrostatic attraction between IgG and the stationary phase, promotes surface-induced unfolding, slows IgG motion, and decreases elution from the column. Our results reveal previously unreported details of antibody structural changes and their influence on macroscale elution profiles.

Keywords: IgG, Ion-exchange chromatography, Surface induced unfolding, 3D single-molecule tracking

Introduction

Antibody-based therapeutics compose one of the fastest-growing sectors in the pharmaceutical industry, with exponentially increasing sales due to excellent therapeutic efficacies.[1-4] However, development of a new antibody-based treatment is expensive, at least partially due to time consuming empirical optimization of separation and purification processes.[5-6] Predictive design of separations would save time and money but requires a quantitative description of antibody interaction with the chromatographic column.[7-8] Antibody purification involves multiple steps, including ion-exchange chromatography (IEX) that may act as a capture step for the specific target molecule, a polishing step, or even in assisting the refolding of unfolded molecules.[9-11] IEX resins have, historically, been thought not to disrupt protein conformation.[12] Conformational changes are one precursor to aggregation, reducing both activity and reliability of the final product.[13] However, recent studies have revealed protein unfolding on the surface of charged resins that are commonly used for IEX.[14-16] The appearance of multiple elution peaks during IEX has been attributed to antibody conformational changes.[17-18] Hydrogen exchange mass spectrometry and Fourier transform infrared spectrometry in combination with size exclusion chromatography have demonstrated that model proteins can undergo conformational changes on strong cation exchangers.[14]

To improve development of antibody separation and purification, it is crucial to understand microscopic details about the motion of denatured molecules, chemical factors that might control molecular structural stability, and the effects of antibody unfolding on IEX elution profiles. Single-protein tracking provides a high spatiotemporal resolution picture of antibody motion in a column, and can connect structural changes to ensemble chromatographic outcomes.[19] By breaking the diffraction limit of light, super-localization methods can identify the position of individual

molecules with ~30 nm resolution, providing precise tracking of interfacial transport.[20-21] Single-molecule methods have already been used to investigate different modes of protein chromatography such as reverse-phase,[22-28] normal-phase,[29-30] and membrane-based separations.[31] A combination of single-molecule techniques and stochastic theory of chromatography has the potential to advance our understanding of antibody IEX by directly connecting elution profiles with single-molecule observables.[32-33]

Traditional 2D single-molecule studies are not ideal for studying realistic interactions with stationary phases.[25, 27, 30-31, 34] Point spread function engineering is one way to encode 3D information in a 2D image.[35-38] The importance of knowledge of analyte motion in three dimensions was previously demonstrated by investigating the influence of the types of particle structure,[39] flow regimes, and dynamics [40] in the column. These examples highlight the advantages of investigating not only the kinetics [33, 41-42] of protein interactions at stationary phases but also protein motion in 3D.

In this study, we combine fast protein liquid chromatography (FPLC) with 3D single-protein tracking and CD spectroscopy to investigate the motion of IgG antibodies as they interact with a model IEX support. We track IgG in the presence of a commonly used weak cation exchanger, carboxymethyl-functionalized agarose (CM agarose), [43] as it adsorbs from a mobile phase under varying salt concentrations. Ensemble chromatograms indicate IgG molecules readily elute at high ionic strengths. Using 3D single-molecule fluorescence microscopy, we correspondingly observe faster IgG motion in the presence of high concentrations of salt. Finally, CD spectra suggest that the negatively charged ligands of the stationary phase can cause surface-induced unfolding of IgG in absence of added salt, while, consistently, higher concentrations of salt prevent such unfolding from occurring.

1. Experimental methods

1.1. Home-built Fast Protein Liquid Chromatography system (FPLC)

All chromatographic results were obtained using a previously reported home-built FPLC (Figure S1).[31] Solutions containing 19 μM IgG from bovine serum (>95%; Sigma) and varied salt concentrations (0.125 M, 0.25 M, 0.5 M, 1 M) were prepared in 10 mM HEPES buffer (Sigma, pH 7.2) and injected into the FPLC using a 1 mL syringe (Becton Dickinson) with an injection volume of 300 μL. A peristaltic pump (Watson-Marlow, 120 Series) was used to create a constant mobile phase flow through the FPLC system at 0.9 mL/min for all experiments. A weak cation exchanger (G-Trap™ CM Agarose Fast Flow, 5 ml column), a weak anion exchanger (G-Trap™ DEAE Agarose Fast Flow, 1 ml column), and affinity column for Immunoglobulins G (G-Trap™ Protein G, 1 ml column) were obtained from G-Bioscience (St. Louis, MO, U.S.A.). To elute IgG from G-Trap Protein G column 0.1 M glycine-HCl, buffer (pH 2.5) was used. Glycine-HCl buffer was prepared by mixing Glycine-HCl (>99%; HPLC, Sigma,) with deionized water and pH was adjusted with sodium hydroxide solution (Macron Fine Chemicals). To quantify the relative amount of IgG molecules eluted from the column, the FPLC detector (Spectrum Chromatography, 280 UV Monitor) measured the eluents absorption of light passing through the flow cell at a single wavelength (280 nm). The signal was converted from current to voltage after collection on a digital recorder (Hantek, 365E) controlled by Hantek 365 software. All components of the FPLC system were connected using silicone tubing (MED-X.D., 0.063" internal diameter).

1.2. Sample preparation

Microscope coverslips (No. 1; VWR, 22 x 22 mm) were sequentially sonicated in cleaning agents: 30 min in soap water (Liquinox 2%), 15 min in deionized water, 15 min in methanol (Sigma, ACS grade), and 15 min in acetone (Sigma, ACS grade). They were then cleaned at 80 °C

for 30 min in a base piranha solution containing 4% (v/v) H_2O_2 (Fisher Scientific) and 13% (v/v) NH_4OH. After rinsing the coverslips with DI water, the coverslips were dried under a stream of nitrogen (Airgas, Ultra Pure). After cleaning, silicon templates (Grace BioLabs, Bend, OR) were attached to each coverslip, and 1 mL of hot 1% (w/w) agarose solution (US Biological, Swampscott, MA) was spun at 3000 rpm in order to exclude any antibody interactions with the glass surface. To make conditions in single-molecule measurements mimic conditions inside the column, we used the following sample preparation routine. We first placed functionalized agarose beads on a microscope cover slip contained within a custom flow chamber (Grace BioLabs). Tubing (Scientific Commodities, 0.03" internal diameter) was connected to the inlet and outlet ports of the chamber (Figure 1A) and a syringe pump was used to create controlled flow of labeled IgG in HEPES buffer (pH 7.2) at 3, 5, 7 or10 μL/min. As a result, directional flow was achieved in the chamber. Flow speed inside the flow chamber was calculated by dividing pump flow rate by chamber cross-section.[44] To take into account the presence of CM agarose beads, we calculated the chamber void volume by weighting the amount of CM agarose used for each sample and then calculating the total volume of agarose beads that occupy the chamber.

1.3. IgG preparation for single-molecule experiments

1.3.1. IgG labeling

IgG was labeled with Alexa Fluor 555 using a protein labeling kit (Molecular Probes). In brief, 50 μl of 1 M sodium bicarbonate buffer (pH 8.3) was added to 500 μl (2 mg/ml in phosphate buffered saline) of IgG. After mixing IgG solution with the Alexa Fluor 555 dye, the reactive mixture was incubated for 1 hour at room temperature. To remove unreacted free dyes, the reaction mixture was exposed to a size exclusion purification resin (BioGel P-30 Fine, Bio-Rad). HEPES buffer (pH 7.2) was used for rinsing during purification.

1.4. 3D single-molecule microscopy

To characterize 3D motion of individual fluorescently labeled IgG inside a chromatographic column, we used 3D single-molecule imaging that combines epi-fluorescence microscopy with double-helix point spread function (DH-PSF) optics[36-37] (Figure 1A) (see SI for details). In DH-PSF imaging, a phase mask is inserted into the Fourier plane in a 4*f* (*f* = 100 mm) imaging geometry converting the conventional Airy disc PSF (Figure 1A, inset left) into a double helix PSF (Figure 1A, inset right) whose relative azimuthal angle encodes the axial position of the emitter (Figure 1B). The lateral (x, y) position of the emitter is determined by finding the midpoint between the two lobes' centers.[45]

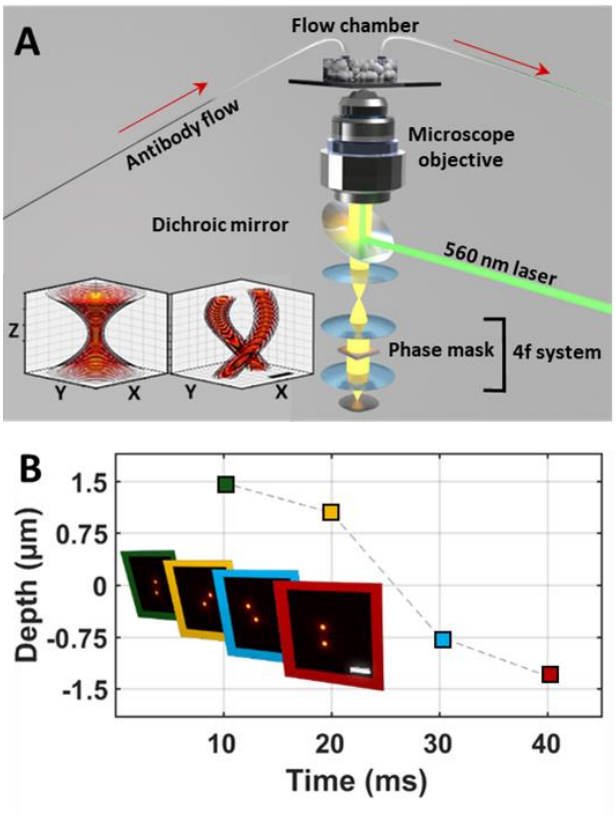

Figure 1 (A) A cartoon of the experimental setup of a wide-field microscope with a DH phase mask. Fluorescently labeled IgG flows through a microfluidic chamber filled with agarose beads. IgG molecules are excited with an epifluorescence-geometry. Fluorescence signal is transmitted through a DH phase mask and is captured by back-illuminated sCMOS camera at the second image plane. The DH phase mask transforms an airy disk PSF (depicted along the focal region) (inset, left) into DH-PSF (inset, right). Relative orientation of the lobes of the DH-PSF (B, inset) allows recovery of the z-position of an emitter (B) in addition, x- and y-coordinates are encoded at the center of the PSF. Images for PSF are simulated. Scale bar: 700 nm

3D tracking information was generated by recording the motion of molecules through a flow chamber packed with agarose beads. We used a custom-developed tracking algorithm[46] (see SI for details) to identify and link positions of single IgGs from frame to frame resulting in 3D trajectories for each molecule that mirror behavior in a chromatographic column.

1.5. Circular Dichroism measurements

CD spectra were acquired using a Jasco J-1500 spectropolarimeter. IgG unlabeled (19 μM) and IgG labeled (0.7 μM) solutions were prepared in 10 mM HEPES buffer (pH 7.2). IgG solutions in the presence of stationary phase were prepared by adding stock solutions of agarose stationary phase (G-Trap™ CM Agarose Fast Flow, G-Trap™ DEAE Agarose Fast Flow and G-Sep™ Agarose 6 Fast Flow). Measurements of each solution were conducted at room temperature in the wavelength range of 190−250 nm with a scan speed of 20 nm/min in a 0.01 cm quartz cuvette, containing 20 μL of solution. Data were obtained in millidegrees and averaged over 10 measurements with a data pitch of 0.1 nm. Millidegrees were converted into molar residue ellipticity ([θ]) using the equation $[\theta] = \frac{\theta}{\mathrm{l}\times\mathrm{N}\times\mathrm{c}\times 10}$, where θ is the ellipticity in degrees, l is the path length of the cuvette in cm, N is the number of amino acids in the antibody, and c is the concentration of the antibody in g/cm^3. Each trace represents 5 scans for each condition. Only spectra from 200 nm to 250 nm were analyzed due to interference at wavelengths below 200 nm caused by the presence of salt.

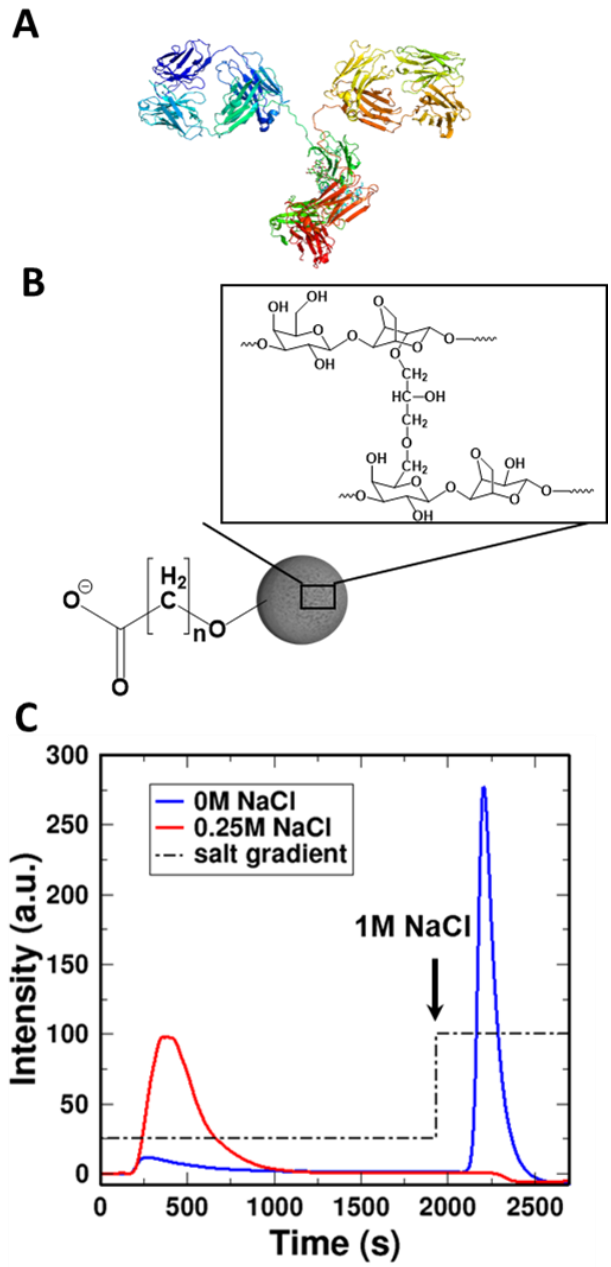

Figure 2 (A) Crystal structure of IgG (PDB:1IGT). (B) Schematic representation of a CM agarose stationary phase that consists of cross-linked agarose beads grafted with carboxymethyl groups. (Inset) The chemical structure of cross-linked agarose. (C) Ensemble experimental results for IgG. Chromatographic elution profiles of IgG on a CM agarose cation-exchange pre-packed column with no salt (blue), and in the presence of 0.25M NaCl (red). The arrow marks the time when a high concentration salt solution was injected.

2. Results and discussion

2.1. Chromatographic retention of IgG

The absence of added salt in the mobile phase decreases the amount of IgG eluted in our home-built FPLC, as expected [47-49] (Figure 2). IgG has an isoelectric point ~7, and thus is typically charge neutral under our experimental conditions [50], while the stationary phase is negatively charged. The structures for IgG and CM agarose are shown in Figure 2A and B, respectively. The average size of the agarose beads is 151.6 ±31.6 µm (see SI for details) which is four orders of magnitude larger than that of the IgG,[51]; thus, multiple individual IgGs may interact with a single agarose bead within the column simultaneously. Figure 2C demonstrates representative elution profiles of IgG alone and with high added salt concentration. Each elution starts with buffer containing either 0 M or 0.25 M NaCl, followed by a step to high salt at 1 M NaCl. The chromatograms show limited elution of IgG without NaCl (Figure 2C, blue), while a peak appears about 2200 s after the addition of 1M NaCl.

Evidently, the IgG is flushed from the column under high NaCl concentration conditions. When eluted with 0.25 M NaCl as an initial condition, a broad retention is observed after 376 s (Figure 2C, red). It is important to note that IgG does completely elute with 0.25 M NaCl, as the area underneath the chromatogram ($(18 \pm 2) \times 10^3$ units) is the same as the total area at 1 M NaCl condition ($(18 \pm 1) \times 10^3$ units). From the equality of the peak areas, we conclude that a great majority of IgG molecules remain in the column in the absence of added salt on the measured time scale, while 0.25 M NaCl is sufficient to elute retained population, although the band is broad. Control experiments (Figure S2) with a broader range of salt concentrations do not show major variations in the retention time of IgG. This control experiment indicates that the electrostatic interactions between the nominally neutral IgG and the stationary phase of the column are not strong and are readily screened.

The observed behavior of IgG elution from the column packed with CM agarose in the presence of NaCl can be explained through the electrostatic shielding effect of salt ions. The addition of NaCl decreases the Debye length of charged ligands leading to decreased interaction between stationary phase and IgG. As a result, the more salt that is added, the weaker electrostatic interactions become. At the experimental conditions used (10 mM HEPES buffer, pH 7.2), IgG is near its isoelectric point, however, due to inherent surface charge heterogeneity,[52] positively charged regions of IgG might interact with the negatively charged stationary phase. Therefore, IgG retention and elution after the addition of NaCl is consistent with an ion exchange process. We hypothesize that variation in IgG retention in the column at different salt conditions can also be explained through other, non-electrostatic, interactions, such as hydrophobic forces or size exclusion related to structural changes. To understand the mechanisms driving the interactions in the present experiments, single-protein tracking and CD spectroscopy were used.

2.2. Super-resolved quasi-chromatography at single-protein tracking conditions

The addition of salt can be shown to increase the velocity of IgG in the mobile phase. Dilute, fluorescently labeled, IgG molecules were pushed through a custom flow chamber (Figure 3A) packed with CM agarose beads extracted from the columns discussed above, mimicking chromatographic conditions. For each salt condition, we capture IgG motion and then reconstruct single-molecule trajectories inside the flow chamber by linking localizations of each molecule in consecutive frames. Representative single IgG trajectories with no added salt and with 0.25 M NaCl are shown in Figure 3B and C, respectively. Time directionality is represented by the color gradient of each trace where the first/last frame of IgG appearance is blue/red. To minimize the influence of sample heterogeneity or any flow effects from sample to sample we measured IgG motion on the same area with and without salt for each sample. Results from analyzing trajectories for both salt conditions evidence larger single frame displacements at higher salt. In the presence of salt, IgG moves more rapidly promoting elution.

Observed IgG motion at the single-molecule level changes linearly with flow rate. In conventional chromatography, it is common to adjust the carrier's flow rate by varying the column head pressure. The flow cell design used here for the microscopic measurements does not allow for any precise pressure changes, so we adjust the pump rate to mimic pressure changes. First, we investigated how the pump flow rate affects IgG motion inside the flow chamber without the addition of salt. IgG molecules were flowed through a chamber (cross section ~0.52 mm^2) packed with CM agarose beads with pump flow rates of 3, 5, 7, and 10 µl/min (see Figure 3D). To demonstrate the dependence of IgG molecules on flow conditions, we calculated the average linear velocity for all detected IgG molecules by extracting the total displacement of each molecule and dividing by the total traveling time for each trajectory captured. Figure 3D (blue crosses) shows

that the dependence of the single-molecule linear velocities on pump flow rate is linear, which is expected for motion under these flow conditions.[53]

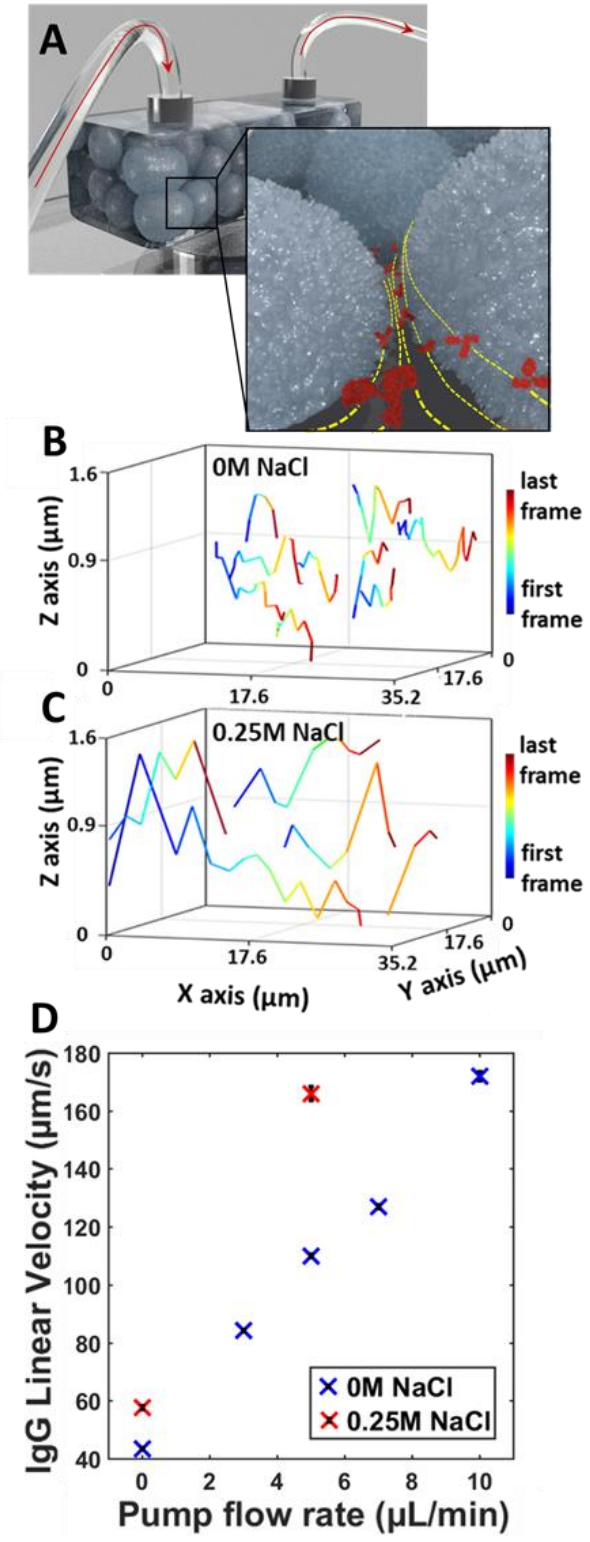

IgG transport near the stationary phase surface is expected to be hindered. Ideally, we would map the flow field in the medium in detail. However, assessing motion under flow is a very complex process and can vary depending on the underlying structure of the stationary phase [54]. As we cannot image the surface of the agarose beads, we will leverage apparent linear velocity as a comparative empirical measure of IgG transport. Knowing pump flow rates and the cross-section of the flow chamber, we can calculate the expected flow speeds inside the chamber for each pump flow rate (Table S1) and compare to observed speeds. Indeed we find that the hypothetical velocities exceed the observed single-molecule linear velocities for IgG (Table S1). Further, the flow chamber is packed with CM agarose beads that likely increase local fluid velocity in the gaps inside the chamber. At the same time, diffusion of IgG in the absence of flow also

Figure 3 (A) Cartoon representation of directional and hindered IgG motion inside the chamber due to proximity to the stationary phase material. Representative trajectories for IgG molecules over the stationary phase without (B) and with (C) salt (0.25 M NaCl). (D) IgG linear velocities without salt (blue) and with salt (red) versus flow rate of the pump

indicated hindered motion within the chamber. Using the Stokes-Einstein relation ($D = \frac{kT}{6\pi\eta R_h}$) with the measured hydrodynamic radius of IgG ($R_h = 6.07 \pm 0.09nm$) from dynamic light scattering (Figure S3), we calculate the diffusion coefficient of freely diffusing IgG as $(4.04\pm0.06)x10^{-7}\ cm^2/s$, matching well with the value reported by others.[55] From freely diffusing IgG measured in our single-molecule system in the absence of flow, we infer a mean diffusion coefficient of $(3.6\pm0.2)x10^{-7}cm^2/s$, which is somewhat smaller. This implies that the observed IgG molecules have hindered motion, likely due to their proximity to the stationary phase material.

To further demonstrate how salt affects IgG motion, we conducted experiments with and without salt in the mobile phase in the absence of flow. When the salt is present in the mobile phase, the observed IgG linear velocity is clearly larger (Figure 3D). From mean-squared-displacement curves (Figure S4), we calculated the mean diffusion coefficients (Table S2). According to the Stokes-Einstein relation, the decreased diffusion coefficient for IgG molecules in the absence of salt suggests a larger hydrodynamic radius. Conversely, the diffusion coefficient with added salt matches better with the published value for IgG without salt [55], pointing to a structural change in IgG due to changing ionic conditions. This is consistent with our earlier hypothesis that antibody structural changes can be a consequence of an ion-exchange process. This process is an important contribution to the dramatically different macroscale separation performance between the two salt conditions.

2.3. Evaluation of IgG structural changes at varying salt conditions

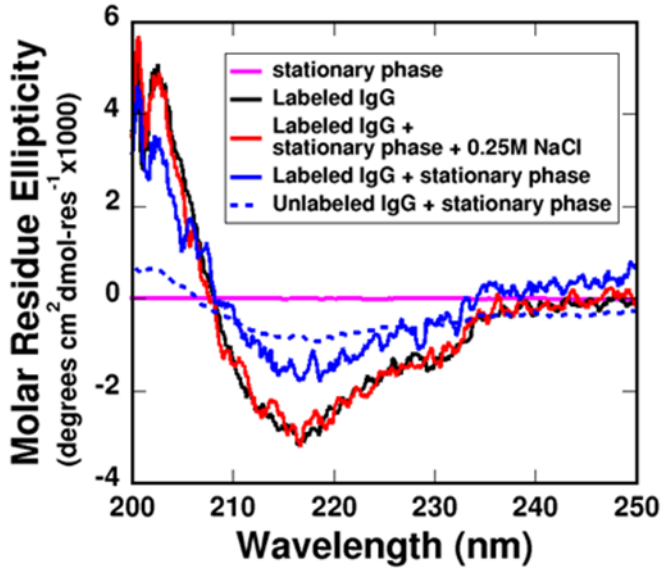

Figure 4 CD spectra of stationary phase (CM agarose), labeled IgG, labeled and unlabeled IgG with CM agarose, and labeled IgG with salt and CM agarose.

We consider further the hypothesis that IgG molecules partially unfold in presence of the CM agarose stationary phase in the absence of salt, influencing overall IgG-stationary phase interactions. Protein structural changes are traditionally considered less significant than electrostatics for IEX, although other interactions, such as hydrophobic effects, can play a significant role. [56] Recent studies have, in fact, demonstrated the influence of protein conformation in IEX resin.[15, 57] To probe IgG structural changes during chromatographic elution and single-molecule experiments, we utilized CD spectroscopy, a widely used tool for identifying changes in protein secondary structure.[58] Free fluorescently labeled IgG (Figure 4, black curve) exhibits a CD spectrum with characteristic features of β-sheets with a minimum at 217 nm and maximum at 202 nm.[59] The residual ellipticity from labeled IgG in the presence of CM agarose stationary phases (Figure 4, blue curve) shows a decrease in amplitude, suggesting some amount of surface-induced unfolding of labeled IgG. Similar decreasing in the amplitude of the signal was observed with unlabeled IgG (Figure 4, dashed blue curve). The addition of salt into the system with CM agarose (Figure 4, red curve) recovers the native conformation of labeled IgG by the current measure. Hence, it is clearly the stationary phase interaction that induces structural change. Protein structural changes increase the hydrodynamic radius of the molecule [60-61], thereby slowing diffusion.[62-63] We hypothesize that

due to electrostatic attraction between IgG and charged stationary phase with no salt in the mobile phase, IgG undergoes surface-induced unfolding resulting in an increase in size, and thus a decrease in diffusion that in turn can slow IgG elution. Meanwhile, salt shields any electrostatic interactions and therefore protects the IgG structure from this perturbation, allowing IgG to fully elute. The dependence of IgG structural preservation on the presence of salt in the mobile phase also corroborates our single-molecule result that the presence of salt increases net transport rates. We also conducted CD experiments with unlabeled IgG used in FPLC experiments to confirm that the addition of Alexa-555 dyes does not alter IgG interactions with stationary phase (Figure S5).

Negatively charged ligands coupled to the CM agarose stationary phase induces some unfolding. We evaluated IgG structure in the presence of agarose, lacking the negatively charged grafted CM ligands. Indeed, the CD spectrum of IgG (Figure S6) in the presence of simple agarose shows no changes in the secondary structure. Next, we evaluated IgG structure in the presence of an *anion* exchange agarose stationary phase, with *positively* charged diethylaminoethyl (DEAE) groups attached to agarose matrix. The CD spectrum of IgG (Figure S7) in the presence of DEAE agarose also shows no changes in the secondary structure. Chromatographic results with the positively charged DEAE agarose column (Figure S8) additionally show that elution time and peak shape are independent of added salt in the mobile phase. Interaction specifically with negatively charged ligands in the cation exchange column is the cause of surface-induced denaturation and retention of IgG inside the CM agarose column.

2.4. Connection between single-molecule and ensemble results

To connect our single-molecule and ensemble results, we compared the average linear velocities for all detected IgG molecules for salt and no salt conditions. In the absence of salt, IgG molecules' linear velocity was 109.7 ± 0.7 μm/sec and the addition of salt increased the velocity

up to 165.9 ± 2.5 μm/sec (Figure 3D). CD results indicate that negatively charged ligands of the CM agarose stationary phase lead to the surface-induced unfolding of IgG without the addition of salt. Previously it has been shown that the IgG multidomain fragment undergoes non-continuous expansion behavior under denaturing conditions.[64] There, the most unfolded conformation was consistent with a diameter more than 3.6 times that of the native conformation, slowing down diffusion significantly, while salt provided a stabilizing effect and prevented the IgG fragments from unfolding. These results are consistent with the observed behavior for IgG here. To eliminate from consideration that agarose bead structural changes with ionic strength could be influencing IgG motion inside the column, we examined the swelling of agarose beads as a function of ionic strength via optical imaging. Figure S9 (A, B) shows that there is no correlation between the diameter of agarose beads and ionic strength of the solution.

We note that our single-molecule experiments have demonstrated slower but significant IgG motion without added salt while macroscale results show exceedingly slow IgG elution. We consider two possible explanations for this apparent discrepancy. The presence of morphological differences inside the commercially available optimized chromatographic column and the quasi-chromatographic flow chamber constructed for single-molecule experiments is a likely suspect. It is commonly accepted that packing microstructure is important for efficient chromatographic performance.[65] Factors such as slurry solvent [66] and concentration [67], packing density [68] and packing method [69] can significantly affect the quality of a separation. Better efficiency, for example, can be achieved by using higher slurry concentrations resulting in suppressing particle size-segregation inside the column.[70] Conversely, there are no special techniques and optimization procedures used to pack the present flow chamber.

Alternatively, the IgG molecules may not be immobilized inside the commercial column but slowly moving without net progress. To evaluate salt-free IgG motion inside this column, we performed two complementary experiments. In the first experiment, we analyzed the peak area measured after a delayed injection of salt. Injection of 1 M NaCl solution was delayed for 15, 180, and 1320 min. Calculated peak areas of eluted IgG after washing the column with 1 M NaCl decreased with increasing time of experiment (Figure S10, black). In the second experiment, we concentrated the effluent from the CM column on a Protein G column which was used as a trap column for slowly moving IgG from CM column. Calculated peak areas of eluted IgG from the Protein G column after washing the CM column with glycine‐HCl buffer (pH 2.5) increased with increasing experiment time(Figure S10, red). Decreasing peak areas for elution with salt and increasing peak areas for elution from Protein G column suggest that IgG is eluting from the column, but in such low concentrations, it falls below the detection threshold of our detector.[71] We can deduce that IgG molecules are not, in fact, immobile but are moving slowly in the absence of salt, at least qualitatively consistent with our single-molecule experiments. The motion of molecules through a column can be described as a random walk between the mobile and stationary phases, where both states play a key role in changing elution curve shape.[72-73]

3. Conclusions

In this work, we advanced our understanding of chromatography by utilizing both ensemble and single-molecule methods. Ensemble chromatograms showed a reduced amount of IgG eluted without salt in the mobile phase. Correspondingly, slower motion of partially denatured IgG molecules in the absence of salt in the presence of the cation exchange media was observed in 3D single-molecule fluorescence microscopy experiments and linked to IgG retention under low salt conditions. This work offers a molecular-scale understanding of IgG structural changes in an IEX

column and its general influence on the elution profile. The above findings have provided molecular scale observations illustrating the consequences of controlling antibody structure and avoiding undesirable unfolding and potential aggregation to achieve desirable macroscale behavior.

Declaration of conflict of interests

The authors declare no competing financial interest.

Author Information

*** Corresponding Author**

Email address: cflandes@rice.edu

T: (713) 348-4232

Rice University, Department of Chemistry, PO Box 1892, MS 60, Houston, TX 77251,

Supplementary materials

Supplementary material associated with this article can be found, in the online version, at:

Experimental details describing IgG concentration measurement, dynamic light scattering, and agarose swelling measurement. Schematics of home-built FPLC system as well as details of the 3D single-molecule microscope. Figures showing additional CD experimental results (three figures) and chromatographic controls (two figures) for different stationary phases; results for DLS measurements; MSD plots for single-molecule results; plots for agarose beads size measurements; calculations for peak areas for eluted IgG with delayed washing and two tables summarizing calculations for IgG velocities and diffusion coefficients.

Acknowledgment

Christy F. Landes thanks the Welch Foundation (Grant C-1787) and the National Science Foundation (NSF CHE-1808382). N.A.M, N.C., and L.D.C.B acknowledge that this material is based upon work supported by the National Science Foundation Graduate Research Fellowship Program (1842494). We thank S. Link and research group for discussions.

References

1. Ecker, D. M.; Jones, S. D.; Levine, H. L., The therapeutic monoclonal antibody market. *MAbs* **2015,** *7*, 9-14.
2. Pavlou, A. K.; Belsey, M. J., The therapeutic antibodies market to 2008. *Eur J Pharm Biopharm* **2005,** *59*, 389-396.
3. Chan, A. C.; Carter, P. J., Therapeutic antibodies for autoimmunity and inflammation. *Nat Rev Immunol* **2010,** *10*, 301-316.
4. Carter, P. J., Potent antibody therapeutics by design. *Nat Rev Immunol* **2006,** *6*, 343-357.
5. Mullin, R., Cost to develop new pharmaceutical drug now exceeds $2.5 B. *Sci. Am.* **2014,** *24*.
6. Walsh, G., Biopharmaceutical benchmarks 2014. *Nat. Biotechnol.* **2014,** *32*, 992.
7. Song, M.; Breneman, C. M.; Bi, J.; Sukumar, N.; Bennett, K. P.; Cramer, S.; Tugcu, N., Prediction of protein retention times in anion-exchange chromatography systems using support vector regression. *J Chem Inf Comput Sci* **2002,** *42*, 1347-1357.
8. Hubbuch, J.; Linden, T.; Knieps, E.; Thömmes, J.; Kula, M. R., Dynamics of protein uptake within the adsorbent particle during packed bed chromatography. *Biotechnol. Bioeng.* **2002,** *80*, 359-368.
9. Follman, D. K.; Fahrner, R. L., Factorial screening of antibody purification processes using three chromatography steps without protein A. *J. Chromatogr. A* **2004,** *1024*, 79-85.
10. Weaver, J.; Husson, S. M.; Murphy, L.; Wickramasinghe, S. R., Anion exchange membrane adsorbers for flow‐through polishing steps: Part II. Virus, host cell protein, DNA clearance, and antibody recovery. *Biotechnol. Bioeng.* **2013,** *110*, 500-510.
11. Li, M.; Zhang, G.; Su, Z., Dual gradient ion-exchange chromatography improved refolding yield of lysozyme. *J. Chromatogr. A* **2002,** *959*, 113-120.
12. Staby, A.; Sand, M.-B.; Hansen, R. G.; Jacobsen, J. H.; Andersen, L. A.; Gerstenberg, M.; Bruus, U. K.; Jensen, I. H., Comparison of chromatographic ion-exchange resins: IV. Strong and weak cation-exchange resins and heparin resins. *J. Chromatogr. A* **2005,** *1069*, 65-77.
13. Wang, W.; Singh, S.; Zeng, D. L.; King, K.; Nema, S., Antibody structure, instability, and formulation. *J. Pharm. Sci.* **2007,** *96*, 1-26.
14. Gillespie, R.; Nguyen, T.; Macneil, S.; Jones, L.; Crampton, S.; Vunnum, S., Cation exchange surface-mediated denaturation of an aglycosylated immunoglobulin (IgG1). *J. Chromatogr. A* **2012,** *1251*, 101-110.
15. Guo, J.; Zhang, S.; Carta, G., Unfolding and aggregation of a glycosylated monoclonal antibody on a cation exchange column. Part I. Chromatographic elution and batch adsorption behavior. *J. Chromatogr. A* **2014,** *1356*, 117-128.
16. Hao, D.; Ge, J.; Huang, Y.; Zhao, L.; Ma, G.; Su, Z., Microscopic insight into role of protein flexibility during ion exchange chromatography by nuclear magnetic resonance and quartz crystal microbalance approaches. *J. Chromatogr. A* **2016,** *1438*, 65-75.
17. Voitl, A.; Butté, A.; Morbidelli, M., Behavior of human serum albumin on strong cation exchange resins: I. Experimental analysis. *J. Chromatogr. A* **2010,** *1217*, 5484-5491.
18. Luo, H.; Macapagal, N.; Newell, K.; Man, A.; Parupudi, A.; Li, Y.; Li, Y., Effects of salt-induced reversible self-association on the elution behavior of a monoclonal antibody in cation exchange chromatography. *J. Chromatogr. A* **2014,** *1362*, 186-193.
19. Shen, H.; Tauzin, L. J.; Baiyasi, R.; Wang, W.; Moringo, N.; Shuang, B.; Landes, C. F., Single particle tracking: from theory to biophysical applications. *Chem. Rev.* **2017,** *117*, 7331-7376.
20. Rust, M. J.; Bates, M.; Zhuang, X., Sub-diffraction-limit imaging by stochastic optical reconstruction microscopy (STORM). *Nat. Methods* **2006,** *3*, 793.
21. Higgins, D. A.; Tran-Ba, K.-H.; Ito, T., Following Single Molecules to a Better Understanding of Self-Assembled One-Dimensional Nanostructures. *J. Phys. Chem. Lett.* **2013,** *4*, 3095-3103.

22. Cooper, J.; Harris, J. M., Fluorescence-correlation spectroscopy study of molecular transport within reversed-phase chromatographic particles compared to planar model surfaces. *Anal. Chem.* **2014,** *86*, 11766-11772.
23. Cooper, J. T.; Harris, J. M., Imaging fluorescence-correlation spectroscopy for measuring fast surface diffusion at liquid/solid interfaces. *Anal. Chem.* **2014,** *86*, 7618-7626.
24. Cooper, J. T.; Peterson, E. M.; Harris, J. M., Fluorescence imaging of single-molecule retention trajectories in reversed-phase chromatographic particles. *Anal. Chem.* **2013,** *85*, 9363-9370.
25. Wirth, M. J.; Swinton, D. J., Single-molecule probing of mixed-mode adsorption at a chromatographic interface. *Anal. Chem.* **1998,** *70*, 5264-5271.
26. Hansen, R. L.; Harris, J. M., Measuring reversible adsorption kinetics of small molecules at solid/liquid interfaces by total internal reflection fluorescence correlation spectroscopy. *Anal. Chem.* **1998,** *70*, 4247-4256.
27. Mabry, J. N.; Skaug, M. J.; Schwartz, D. K., Single-molecule insights into retention at a reversed-phase chromatographic interface. *Anal. Chem.* **2014,** *86*, 9451-9458.
28. Wirth, M. J.; Legg, M. A., Single-molecule probing of adsorption and diffusion on silica surfaces. *Annu. Rev. Phys. Chem.* **2007,** *58*, 489-510.
29. Kang, S. H.; Shortreed, M. R.; Yeung, E. S., Real-time dynamics of single-DNA molecules undergoing adsorption and desorption at liquid− solid interfaces. *Anal. Chem.* **2001,** *73*, 1091-1099.
30. Xu, X.-H. N.; Yeung, E. S., Long-range electrostatic trapping of single-protein molecules at a liquid-solid interface. *Science* **1998,** *281*, 1650-1653.
31. Moringo, N. A.; Bishop, L. D.; Shen, H.; Misiura, A.; Carrejo, N. C.; Baiyasi, R.; Wang, W.; Ye, F.; Robinson, J. T.; Landes, C. F., A mechanistic examination of salting out in protein–polymer membrane interactions. *Proc Natl Acad Sci U S A* **2019,** *116*, 22938-22945.
32. Kisley, L.; Chen, J.; Mansur, A. P.; Shuang, B.; Kourentzi, K.; Poongavanam, M.-V.; Chen, W.-H.; Dhamane, S.; Willson, R. C.; Landes, C. F., Unified superresolution experiments and stochastic theory provide mechanistic insight into protein ion-exchange adsorptive separations. *Proc Natl Acad Sci U S A* **2014,** *111*, 2075-2080.
33. Kisley, L.; Chen, J.; Mansur, A. P.; Dominguez-Medina, S.; Kulla, E.; Kang, M. K.; Shuang, B.; Kourentzi, K.; Poongavanam, M. V.; Dhamane, S.; Willson, R. C.; Landes, C. F., High ionic strength narrows the population of sites participating in protein ion-exchange adsorption: a single-molecule study. *J. Chromatogr. A* **2014,** *1343*, 135-42.
34. Moringo, N. A.; Shen, H.; Bishop, L. D.; Wang, W.; Landes, C. F., Enhancing analytical separations using super-resolution microscopy. *Annu. Rev. Phys. Chem.* **2018,** *69*, 353-375.
35. Pavani, S. R. P.; Greengard, A.; Piestun, R., Three-dimensional localization with nanometer accuracy using a detector-limited double-helix point spread function system. *Appl. Phys. Lett.* **2009,** *95*, 021103.
36. Pavani, S. R. P.; Piestun, R., Three dimensional tracking of fluorescent microparticles using a photon-limited double-helix response system. *Opt. Express* **2008,** *16*, 22048-22057.
37. Pavani, S. R. P.; Thompson, M. A.; Biteen, J. S.; Lord, S. J.; Liu, N.; Twieg, R. J.; Piestun, R.; Moerner, W., Three-dimensional, single-molecule fluorescence imaging beyond the diffraction limit by using a double-helix point spread function. *Proc Natl Acad Sci U S A* **2009,** *106*, 2995-2999.
38. Wu, H.; Schwartz, D. K., Nanoparticle Tracking to Probe Transport in Porous Media. *Acc. Chem. Res.* **2020,** *53*, 2130-2139.
39. Daneyko, A.; Hlushkou, D.; Baranau, V.; Khirevich, S.; Seidel-Morgenstern, A.; Tallarek, U., Computational investigation of longitudinal diffusion, eddy dispersion, and trans-particle mass transfer in bulk, random packings of core–shell particles with varied shell thickness and shell diffusion coefficient. *J. Chromatogr. A* **2015,** *1407*, 139-156.

40. Tallarek, U.; Vergeldt, F. J.; As, H. V., Stagnant mobile phase mass transfer in chromatographic media: intraparticle diffusion and exchange kinetics. *J. Phys. Chem. B* **1999,** *103*, 7654-7664.
41. Moringo, N. A.; Shen, H.; Tauzin, L. J.; Wang, W.; Landes, C. F., Polymer Free Volume Effects on Protein Dynamics in Polystyrene Revealed by Single-Molecule Spectroscopy. *Langmuir* **2020,** *36*, 2330-2338.
42. Skaug, M. J.; Mabry, J.; Schwartz, D. K., Intermittent molecular hopping at the solid-liquid interface. *Phys. Rev. Lett.* **2013,** *110*, 256101.
43. Boschetti, E., Advanced sorbents for preparative protein separation purposes. *J. Chromatogr. A* **1994,** *658*, 207-236.
44. Riva, C. E.; Grunwald, J. E.; Sinclair, S. H.; Petrig, B., Blood velocity and volumetric flow rate in human retinal vessels. *Investigative ophthalmology & visual science* **1985,** *26*, 1124-1132.
45. Wang, W.; Shen, H.; Moringo, N. A.; Carrejo, N. C.; Ye, F.; Robinson, J. T.; Landes, C. F., Super-temporal resolved microscopy reveals multistep desorption kinetics of α-lactalbumin from nylon. *Langmuir* **2018**.
46. Shuang, B.; Chen, J.; Kisley, L.; Landes, C. F., Troika of single particle tracking programing: SNR enhancement, particle identification, and mapping. *Phys. Chem. Chem. Phys.* **2014,** *16*, 624-34.
47. Hahn, R.; Schulz, P.; Schaupp, C.; Jungbauer, A., Bovine whey fractionation based on cation-exchange chromatography. *J. Chromatogr. A* **1998,** *795*, 277-287.
48. Goyon, A.; McDonald, D.; Fekete, S.; Guillarme, D.; Stella, C., Development of an innovative salt-mediated pH gradient cation exchange chromatography method for the characterization of therapeutic antibodies. *J. Chromatogr. B* **2020,** *1160*, 122379.
49. Fekete, S.; Beck, A.; Fekete, J.; Guillarme, D., Method development for the separation of monoclonal antibody charge variants in cation exchange chromatography, Part I: salt gradient approach. *J. Pharm. Biomed. Anal.* **2015,** *102*, 33-44.
50. Palecek, S. P.; Zydney, A. L., Intermolecular electrostatic interactions and their effect on flux and protein deposition during protein filtration. *Biotechnol. Progr.* **1994,** *10*, 207-213.
51. Jøssang, T.; Feder, J.; Rosenqvist, E., Photon correlation spectroscopy of human IgG. *J. Protein Chem.* **1988,** *7*, 165-171.
52. Boswell, C. A.; Tesar, D. B.; Mukhyala, K.; Theil, F.-P.; Fielder, P. J.; Khawli, L. A., Effects of charge on antibody tissue distribution and pharmacokinetics. *Bioconjugate Chem.* **2010,** *21*, 2153-2163.
53. Cramers, C.; Rijks, J.; Schutjes, C., Factors determining flow rate in chromatographic columns. *Chromatographia* **1981,** *14*, 439-444.
54. Hlushkou, D.; Piatrusha, S.; Tallarek, U., Impact of diffusion on transverse dispersion in two-dimensional ordered and random porous media. *Physical Review E* **2017,** *95*, 063108.
55. Pokrić, B.; Pučar, Z., The two-cross immunodiffusion technique: diffusion coefficients and precipitating titers of IgG in human serum and rabbit serum antibodies. *Anal. Biochem.* **1979,** *93*, 103-114.
56. Yu, L.; Zhang, L.; Sun, Y., Protein behavior at surfaces: orientation, conformational transitions and transport. *J. Chromatogr. A* **2015,** *1382*, 118-134.
57. Guo, J.; Carta, G., Unfolding and aggregation of monoclonal antibodies on cation exchange columns: effects of resin type, load buffer, and protein stability. *J. Chromatogr. A* **2015,** *1388*, 184-194.
58. Ranjbar, B.; Gill, P., Circular dichroism techniques: biomolecular and nanostructural analyses‐a review. *Chemical biology & drug design* **2009,** *74*, 101-120.
59. Thakur, R.; Das, A.; Sharma, V.; Adhikari, C.; Ghosh, K. S.; Chakraborty, A., Interaction of different prototropic species of an anticancer drug ellipticine with HSA and IgG proteins: multispectroscopic and molecular modeling studies. *PCCP* **2015,** *17*, 16937-16946.

60. Adel, A.; Nadia, M.; Mohamed, O.; Abdelhafidh, G., Study of thermally and chemically unfolded conformations of bovine serum albumin by means of dynamic light scattering. *Mater. Sci. Eng. C* **2008,** *28*, 594-600.
61. Uversky, V. N., Use of fast protein size-exclusion liquid chromatography to study the unfolding of proteins which denature through the molten globule. *Biochemistry* **1993,** *32*, 13288-13298.
62. Molchanov, S.; Faizullin, D. A.; Nesmelova, I. V., Theoretical and Experimental Investigation of the Translational Diffusion of Proteins in the Vicinity of Temperature-Induced Unfolding Transition. *J. Phys. Chem. B* **2016,** *120*, 10192-10198.
63. Nesmelova, I. V.; Melnikova, D. L.; Ranjan, V.; Skirda, V. D., Translational diffusion of unfolded and intrinsically disordered proteins. *Prog. Mol. Biol. Transl. Sci.* **2019,** *166*, 85-108.
64. Guo, L.; Chowdhury, P.; Glasscock, J. M.; Gai, F., Denaturant-induced expansion and compaction of a multi-domain protein: IgG. *J. Mol. Biol.* **2008,** *384*, 1029-1036.
65. Martinez, A.; Knaub, K.; Monter, M.; Hekmat, D.; Weuster‐Botz, D., Improved packing of preparative biochromatography columns by mechanical vibration. *Biotechnol. Progr.* **2020,** *36*, e2950.
66. Blue, L. E.; Jorgenson, J. W., 1.1 µm superficially porous particles for liquid chromatography. Part I: synthesis and particle structure characterization. *J. Chromatogr. A* **2011,** *1218*, 7989-7995.
67. Bruns, S.; Franklin, E. G.; Grinias, J. P.; Godinho, J. M.; Jorgenson, J. W.; Tallarek, U., Slurry concentration effects on the bed morphology and separation efficiency of capillaries packed with sub-2 µm particles. *J. Chromatogr. A* **2013,** *1318*, 189-197.
68. Stanley, B. J.; Foster, C. R.; Guiochon, G., On the reproducibility of column performance in liquid chromatography and the role of the packing density. *J. Chromatogr. A* **1997,** *761*, 41-51.
69. Godinho, J. M.; Reising, A. E.; Tallarek, U.; Jorgenson, J. W., Implementation of high slurry concentration and sonication to pack high-efficiency, meter-long capillary ultrahigh pressure liquid chromatography columns. *J. Chromatogr. A* **2016,** *1462*, 165-169.
70. Reising, A. E.; Godinho, J. M.; Jorgenson, J. W.; Tallarek, U., Bed morphological features associated with an optimal slurry concentration for reproducible preparation of efficient capillary ultrahigh pressure liquid chromatography columns. *J. Chromatogr. A* **2017,** *1504*, 71-82.
71. Bishop, L. D.; Misiura, A.; Moringo, N. A.; Landes, C. F., Unraveling peak asymmetry in chromatography through stochastic theory powered Monte Carlo simulations. *J. Chromatogr. A* **2020**, 461323.
72. Giddings, J. C., The random downstream migration of molecules in chromatography. *J. Chem. Educ.* **1958,** *35*, 588.
73. Giddings, J. C.; Eyring, H., A molecular dynamic theory of chromatography. *J. Phys. Chem.* **1955,** *59*, 416-421.

TOC figure